Lecture 4: Experiments and Numerics

E. J. Hinch

1 Experiments

In this section we discuss experimental approaches to characterizing materials and assessing the behavior of flowing materials. Standard apparatuses used to determine fluid rheology were described in section 3 of Lecture 1. Here we emphasize practical problems in measuring the rheology of non-Newtonian fluids, the importance of using standard fluids, and methods for observing flow properties.

1.1 Materials

What is a complete rheological description? Measuring the shear viscosity, normal stresses and elastic modulus in shear flow is not sufficient to describe a fluid, as two fluids may be similar in these characteristics and yet have distinct behavior in extensional flow. It is important to document experimental details carefully, including measurement technique, fluid preparation and molecular weight distributions, so that others can reproduce the results. To this end, rheologists study standard fluids. Meissner [1] coordinated a project to examine low density polyethylene fluids. In more recent years, there has been a transition from the use of hot melts to cold solutions as standard fluids for logistical ease.

An example of a modern standard fluid is the M1 ('magic') fluid which consists of 0.244 % polyisobutylene (molecular weight 3.8×10^6 g/mol) and 7% kerosene in polybutene. The M1 fluid is a Boger fluid, that is, one which has a shear viscosity that is approximately independent of shear rate, thus allowing a separation of shear and elastic effects. There is good agreement amongst different shear rheometers in the measurements of shear viscosity of the M1 fluid. However a series of extensional viscosity measurements demonstrates that different measurement techniques can lead to a range of extensional viscosities [2] (up to four orders of magnitude; see figure 2 from Lecture 1. A rational explanation of this phenomenon will be given in Lecture 9.

1.1.1 Practical problems

There are many experimental difficulties in measuring the properties of non-Newtonian fluids. These include:

- Flow instabilites in Couette and cone-and-plate apparatuses can produce a jump in torque that may be erroneously interpreted as an increase in viscosity.

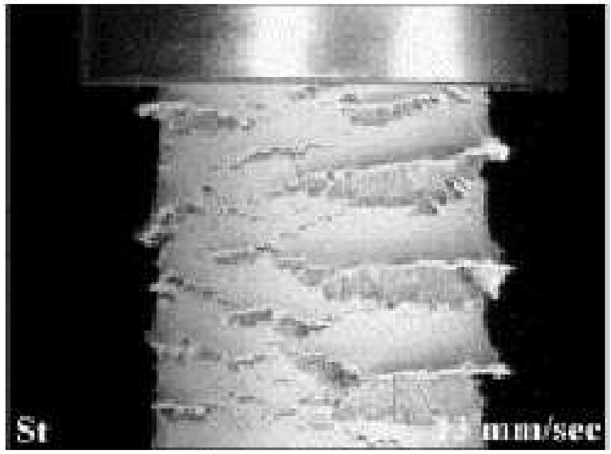

Figure 1: Stick-slip from flow of a mixture of clay powder and oil through a 20 mm diameter steel dye at 13 mm/s [4].

- The no-slip boundary condition at walls is generally assumed but is not always valid (figure 1).
- There can be slipping along internal layers, known as shear banding. Rheometers can be designed to observe this phenomena to avoid misinterpretations.
- Friction from shearing viscous fluids increases temperatures in the fluids, which causes a reduction in fluid viscosity.
- Phase-separation and crystallisation will cause changes in rheological properties. The standard S1 ('silly') fluid (5% polyisobutylene in decalin [3] by weight) has been problematic because it tends to phase separate.
- Degradation of the fluid due to UV radiation, bio-organisms or mechanical breaking of polymers by the flow itself (*e.g.*, figure 2).

1.2 Observations

Standard methods of flow observation include direct visualisation, laser doppler anemometry and particle image velocimetry. Fluid properties and flow characteristics can also be inferred from measurements of fluid fluxes and normal stresses for flow through a simple geometry such as flow through a pipe. There are however complications associated with this technique. There is a large pressure drop at pipe entry, an effect that can be accounted for by using a range of pipe lengths and extrapolating the data to an infinite pipe. Additionally there is an error associated with measuring normal stresses using pressure taps in the walls, because flow past the hole creates normal stresses.

Visualization may be complemented by assessing stresses from flow-induced anisotropy in the optical index of refraction of the fluid (birefringence). When plane-polarized monochromatic light passes through the fluid and then through a second polarizer, the birefringence

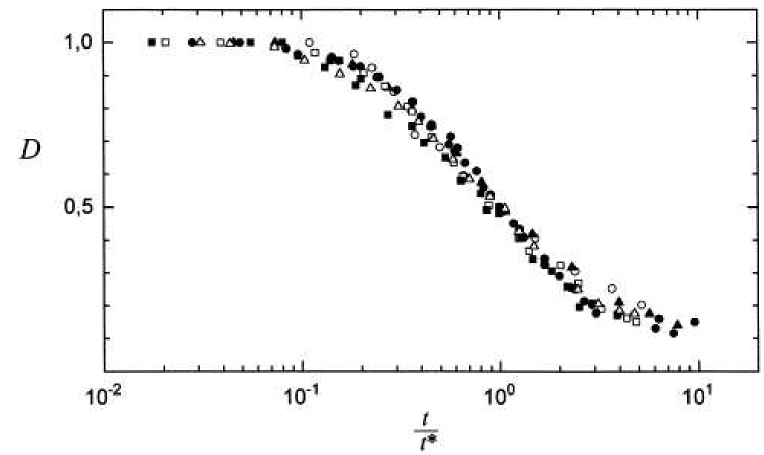

Figure 2: Plot showing drag reduction for aqueous PEO solutions with time related to mechanical degredation of polymers. The symbols correspond to experiments at different Reynolds numbers ($2.0 \times 10^{-5} < Re < 18.1 \times 10^{-5}$). t is the residence time of the solution in the flow and t^* is the half-degradation time [5].

of the fluid causes constructive and destructive interference fringes (figure 3) from which stress contours are deduced (figure 4). A linear relationship between stress and index of refraction (n) is sometimes assumed,

$$\sigma = c\Delta n, \tag{1}$$

where c, the stress optical coefficient, is a constant determined from a simple test flow. For qualitative assessment (1) is not required however the quantitative application of this technique depends on the validity of the stress optical law. This law may fail because birefringence measures bond alignment and not the magnitude of the stretching. This is particulary problematic in strong extensional flows.

Failure of the stress-optical law was demonstrated by [7] with simultaneous measurements of birefringence and extensional stress of polymer solutions in a filament stretching rheometer. The data indicate a non-linear relationship between stress and birefringece. Furthermore, stress relaxation was faster than birefringence relaxation, leading to a hysteresis in the stress optical law (figure 5).

2 Numerics

2.1 Discretization

There are three methods of discretisation which are commonly used in the numerical solution of non-Newtonian fluid flow problems. These are finite element, spectral and finite difference methods. Finite element techniques are good for problems with complex geometries, and as solvers for elliptic equations. Spectral methods are very accurate but only work for periodic geometries such as a wavy-wall tube. They are often used for turbulent drag problems. Finite difference methods are relatively simple and are most easily applied to mappable

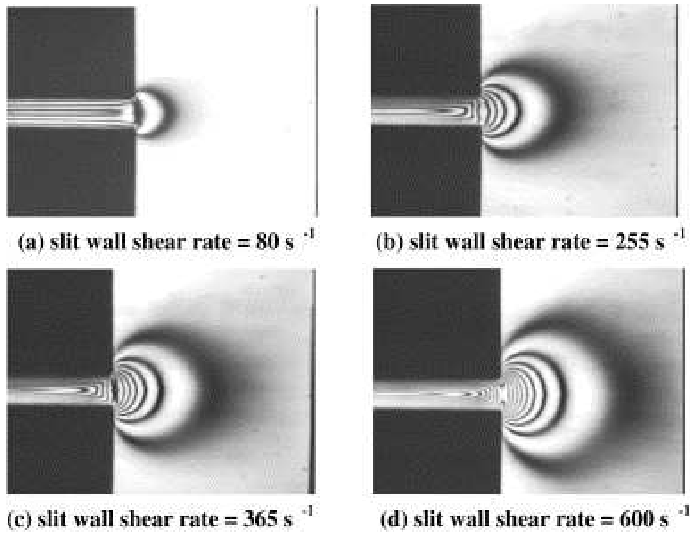

Figure 3: Photographs of fringe patterns for fluid flowing into a slit for a range of shear rates. Dark fringes are areas of destructive interference and each additional fringe indicates that the slow ray is an additional wavlength behind the fast light ray. From [6]

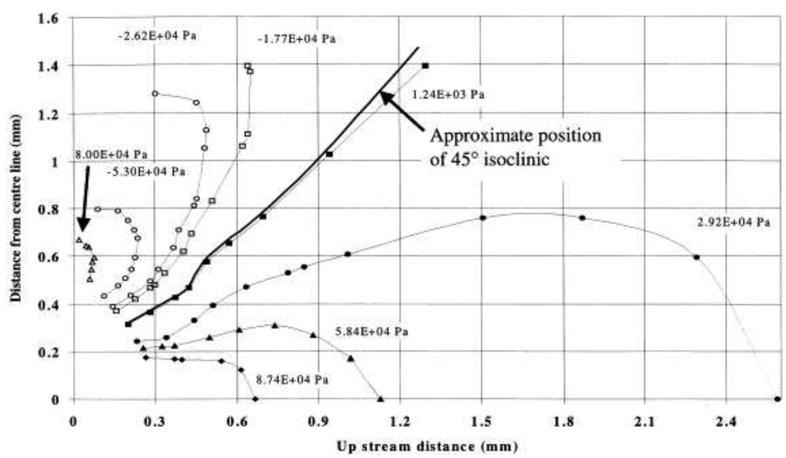

Figure 4: The first normal stress contours corresponding to the flow shown in Figure 3, part (b).

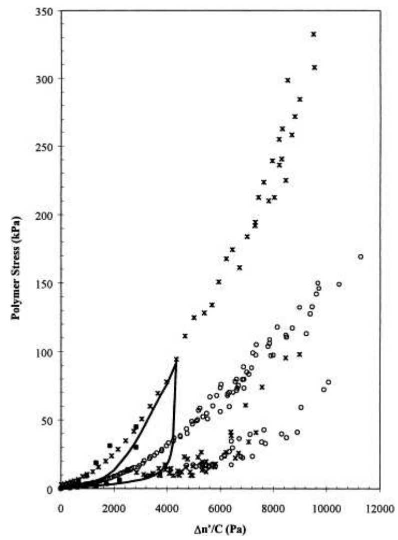

Figure 5: Stress versus birefringence for extensional flow and subsequent relaxation at a range of Weissenberg numbers; asterisk: Wi = 41.7, circle: Wi = 16.8, square: Wi = 2.84, line: conformation dependent FENE model with Wi = 2.84.

geometries (*i.e.,* domains that can be mapped onto a quadrilateral grid). We include only a brief overview of each of these methods. For further details, see *e.g.* [8].

2.1.1 Finite Elements

The domain is divided into a grid of triangular or quadrilateral elements, (note that use of a triangular grid can lead to difficulties with list processing associated with the storing of neighbouring elements). The unknown fields (such as velocity) are represented by a sum (over the elements) of the product of known functions, ϕ_i, and unknown amplitudes, f_i,

$$\mathbf{u}(\mathbf{x}) = \sum^{N} f_i \, \phi_i(\mathbf{x}), \tag{2}$$

where ϕ_i are referred to as test functions. These summation representations are substituted into the governing equations, and then on projection we have

$$\int \left(\rho \frac{\mathrm{D}\mathbf{u}}{\mathrm{D}t} + \nabla p - \mu \nabla^2 \mathbf{u} - \nabla \cdot \sigma^{elast} \right) \cdot \phi_s(\mathbf{x}) \, dV = 0, \quad \text{for } s = 1, 2, ...N. \tag{3}$$

By requiring the above relation to hold, we obtain a set of ordinary differential equations for the functions f_i. These can be solved easily (*e.g.* using a Runge-Kutta scheme) to find the f_i and hence the unknown fields.

2.1.2 Spectral Methods

Similar to the finite element method, the spectral representation of flows is a summation of the product of an unknown amplitude with a known basis function (such as Fourier or

Chebyshev modes) so

$$f(x) = \sum^{N} f_n \, e^{inx}. \tag{4}$$

The elegance of this method lies in the fact that spatial derivatives of (4) become multiplications, which are numerically simple to perform, and the error term in such a representation is exponentially small,

$$f'(x) = \sum^{N} f_n in \, e^{inx} + O(e^{-N}). \tag{5}$$

A disadvantage of this method is that the product of two functions requires summing over cross terms which is computationally expensive,

$$f(x)g(x) = \sum_{n}^{N} \sum_{k}^{N} f_k \, g_{n-k} e^{inx}. \tag{6}$$

In order to avoid this expense, pseudo-spectral methods are used instead. This method calculates the derivatives using (5) but the product of functions is calculated with the actual function values (using Fast Fourier transforms to switch between the two). To avoid aliasing it is common to remove the top third of the spectrum (for quadratic nonlinearities). Spectral methods are ideal for periodic boundaries but cannot represent discontinuities in the flow very well because the basis functions are smooth.

2.1.3 Finite Difference Methods

Finite difference methods are widely employed in modeling fluid dynamics problems. This method involves a coordinate grid so the labelling and interaction of nodes is straightforward. The equations are generally discretised using a second-order central differencing scheme. For example, the second derivative is approximated by

$$f'' \approx \frac{f(x+h) - 2f(x) + f(x-h)}{h^2}. \tag{7}$$

It is important to note that the discretization process can sometimes lead to errors. For example the finite difference expression for the divergence of radial flow is not the same as the analytical expression,

2.2 Benchmark numerical cases

Solutions from benchmark problems are used for testing numerical codes. Some common examples are shown in figure 6 below.

2.3 Pressure

The pressure in two-dimensional calculations for Newtonian fluids can be avoided by taking the curl of the momentum equation to obtain the vorticity equation. However this is not possible for calculations involving non-Newtonian fluids because all components of the stress tensor are required to give an accurate description of the flow.

Sphere in a tube:

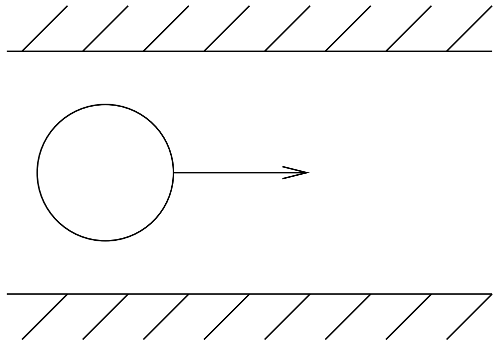

Dominated by shear

Contraction:

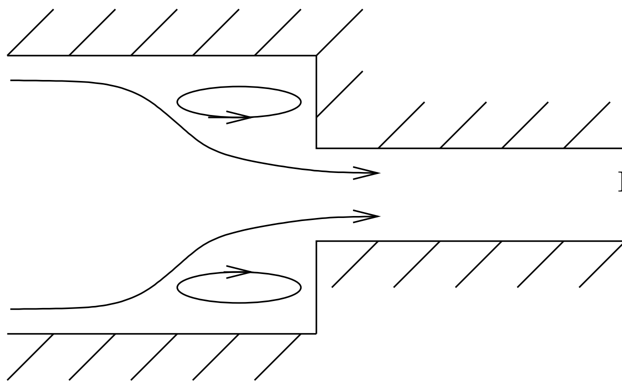

Difficult sharp corner

Journal bearing:

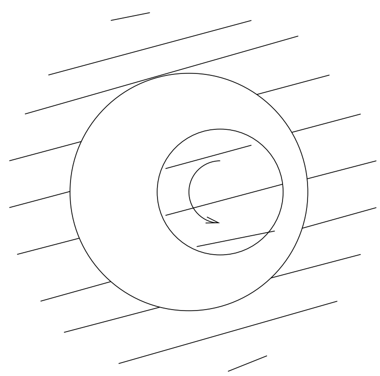

Good for spectral methods

Wavy-wall pipe:

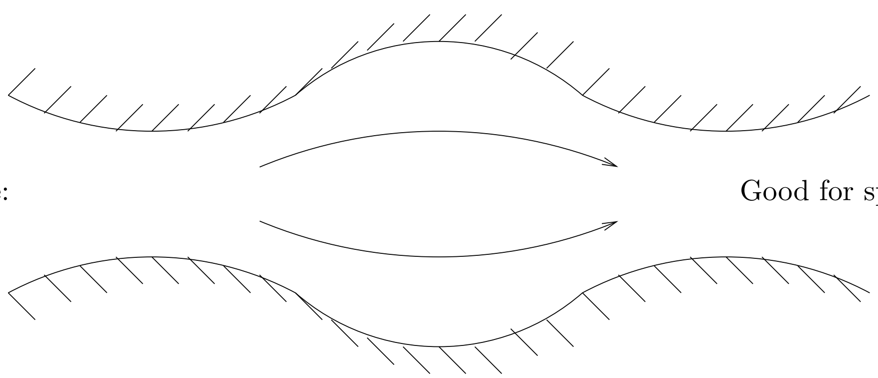

Good for spectral methods

Figure 6: Benchmark problems for testing numerical code.

2.3.1 Fractional step with pressure projection

Consider the pressure equation (found by taking the divergence of the momentum equation),

$$\nabla^2 p = \nabla \cdot \left[-\rho \frac{\mathrm{D}\mathbf{u}}{\mathrm{D}t} + \nabla \cdot (\sigma^{\mathrm{visc}} + \sigma^{\mathrm{elast}}) \right]. \tag{8}$$

When solving numerically for the pressure, incompressibility is usually satisfied only to within a small error, so that

$$\nabla \cdot \mathbf{u} \approx 0. \tag{9}$$

Over many timesteps these small errors can accumulate, leading to a significant error. This problem can be reduced using a fractional step with pressure projection. This numerical technique (used with finite differencing, finite element and spectral methods) finds an approximate solution $\mathbf{u}^*$ and then makes a correction which removes the error in the incompressibilty condition and guarantees that $\nabla \cdot \mathbf{u} = 0$ exactly.

The fractional step uses $\mathbf{u}^*$ found by solving

$$\frac{\mathbf{u}^* - \mathbf{u}^n}{\Delta t} = -(\rho \mathbf{u} \cdot \nabla \mathbf{u})^n + \nabla \cdot (\sigma^{visc} + \sigma^{elast})^n, \tag{10}$$

with the no-slip boundary condition and then the pressure projection gives the solution for the next timestep,

$$\mathbf{u}^{n+1} = \mathbf{u}^* - \Delta t \nabla p^{n+1}. \tag{11}$$

Note therefore that

$$\nabla \cdot \mathbf{u}^{n+1} = \nabla \cdot \mathbf{u}^* - \Delta t\, \nabla^2 p^{n+1} = \nabla \cdot \mathbf{u}^* - \nabla \cdot \mathbf{u}^* = 0. \tag{12}$$

The disadvantage of this technique is that the no-slip boundary condition is not exactly satisifed by $\mathbf{u}^{n+1}$.

2.3.2 Fractional step with pressure update

The method described above can be refined by using a fractional step with a pressure update. This includes the pressure term explicitly in the calculations, so adjustments are made to the pressure at the previous time, as opposed to recalculating the pressure field at each timestep. This method is much better at handling the boundary conditions and leads to a closer approximation to the no-slip condition.

The velocity at the fractional step, $\mathbf{u}^*$ is given by

$$\frac{\mathbf{u}^* - \mathbf{u}^n}{\Delta t} = -\nabla p^{n-\frac{1}{2}} + \left[-\rho \mathbf{u} \cdot \nabla \mathbf{u} + \nabla \cdot \sigma^{\mathrm{elast}} \right]^{n+\frac{1}{2}} + \left[\nabla \cdot \sigma^{\mathrm{visc}} \right]^{n+\frac{1}{2}}, \tag{13}$$

where $p^{n-1/2}$ is the pressure at the last step. Then the non-zero divergence of $\mathbf{u}^*$ is given by

$$\nabla \cdot \mathbf{u}^* = \Delta t\, \nabla^2 \delta p^{n+\frac{1}{2}}. \tag{14}$$

The solution (including the pressure field) is then updated by

$$\mathbf{u}^{n+1} = \mathbf{u}^* - \Delta t\, \nabla \delta p^{n+\frac{1}{2}}, \tag{15}$$

$$p^{n+\frac{1}{2}} = p^{n-\frac{1}{2}} + \delta p^{n+\frac{1}{2}}. \tag{16}$$

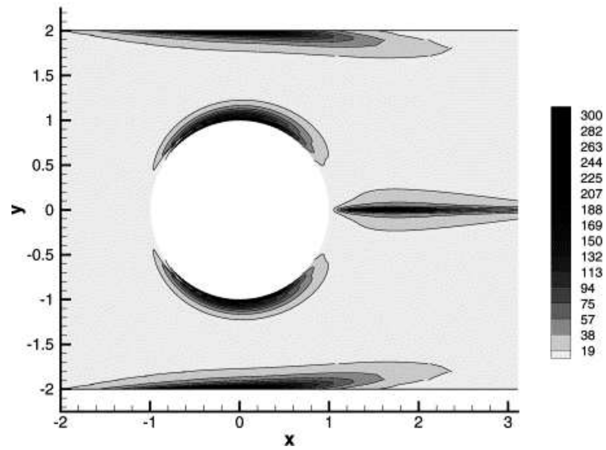

Figure 7: Contours of the configuration tensor component $< QQ >_{xx}$ around a cylinder for flow of an Oldroyd-B fluid through a linear array of cylinders with $De = 1$. From [10].

2.3.3 Staggered grids

Central differencing can lead to spurious pressure modes (oscillations on the scale of the grid). In finite difference techniques these can be avoided by using a staggered grid, in which different fields are held on different points, (*e.g.* velocities on the midpoints of cells boundaries, shear stresses on the corners and momentum terms at the cell center). However, a staggered grid is not possible with finite element models. This leaves an essential difficulty in such schemes.

2.4 Elliptic and hyperbolic parts

The elliptic pressure equation is relatively easily solved. However the stress equation is a hyperbolic partial differential equation and there is no easy method of solution. With a finite difference code, the method of characteristics can be employed (using the streamlines as the characteristics). An alternative is 'black box magic' such as the code MINMOD, which uses second order discretization over the domain except in the vicinity of shocks where the discretization is first-order. For finite-element methods an upwinding technique can offer a method of solution, however this generates large numerical diffusion. Alternatively a lagrangian grid can be used, so that the grid and the elements defined on it travel along with the flow, such as that employed by [9].

2.5 Numerical Problems

There are a number of problems which develop when computing non-Newtonian flows. Convergence tests are often neglected and numerical instabilities can develop when simulating flows with sharp corners, interfaces between shear layers, and thin layers of high stress (*e.g.* 7). More grid resolution is needed in these areas, however it is computationally expensive.

A limitation of the Upper Convective Maxwell and Oldroyd-B models is that there appear to be no solutions for large Deborah numbers (high strain rates). For flow past a sphere in a tube, the maximum Deborah numbers are $De_{max} = 2.17$ and $De_{max} = 1.28$ for the UCM and Oldroyd-B models, respectively [11]. At greater than these critical Deborah numbers there is a region in which the extensional viscosity is negative. The FENE model (Finite Extension Nonlinear Elasticity), overcomes this problem and is sucessful up to $De \approx 100$ (see Lecture 2).

Notes by Alison Rust and Julia Mullarney

References

[1] J. Meissner, "Basic parameters, melt rheology, processing and end-use properties of three similar low density polyethylene samples," Pure Appl. Chem. **42**, 553 (1975).

[2] R. A. Keiller, "Modelling of the extensional flow of the m1 fluid with the oldroyd equation," J. Non-Newtonian Fluid Mech. **42**, 49 (1992).

[3] N. E. Hudson and J. Ferguson, "The anomalous shear flow properties of s1," J. Non-Newtonian Fluid Mech. **52**, 105 (1994).

[4] O. L. Kulikov and K. Hornung, "A simple geometrical solution to the surface fracturing problem in extrusion processes," J. Non-Newtonian Fluid Mech. **98**, 107 (2001).

[5] V. N. Kalashnikov, "Degradation accompanying turbulent drag reduction by polymer additives," J. Non-Newtonian Fluid Mech. **103**, 105 (2002).

[6] M. T. Martyn, C. Nakason, and P. D. Coates, "Stress measurements for contraction flows of viscoelastic polymer melts," J. Non-Newtonian Fluid Mech. **91**, 123 (2000).

[7] T. Sridhar, D. A. Nguyen, and G. G. Fuller, "Birefringence and stress growth in uniaxial extension of polymer solutions," J. Non-Newtonian Fluid Mech. **90**, 299 (2000).

[8] R. Peyret and T. D. Taylor, *Computational Methods for Fluid Flow* (Springer-Verlag, New York, 1983).

[9] P. Szabo, J. M. Rallison, and E. J. Hinch, "Start-up of flow of a fene-fluid through a 4:1:4 constriction in a tube," J. Non-Newtonian Fluid Mech. **72**, 73 (1997).

[10] A. E. Caola, Y. L. Joo, R. C. Armstrong, and R. A. Brown, "Highly parallel time integration of viscoelastic flows," J. Non-Newtonian Fluid Mech. **100**, 191 (2001).

[11] Y. Fan, "Limiting behavior of the solutions of a falling sphere in a tube filled with viscoelastic fluids," J. Non-Newtonian Fluid Mech. **110**, 77 (2003).